Reaction of NO with the Reduced R2 Protein of Ribonucleotide Reductase from *Escherichia coli*†

Charlene J. Haskin,‡ Natarajan Ravi,§ John B. Lynch,‡,|| Eckard Münck,*,§ and Lawrence Que, Jr.*,‡

Department of Chemistry, University of Minnesota, Minneapolis, Minnesota 55455, and Department of Chemistry, Carnegie Mellon University, Pittsburgh, Pennsylvania 15213

Received March 31, 1995; Revised Manuscript Received July 10, 1995⊗

ABSTRACT: The active R2 protein of ribonucleotide reductase from *Escherichia coli* contains a catalytically essential tyrosine radical at position 122 (Tyr_{122}•) that is formed during the reaction of dioxygen with the nearby diiron(II) center. To gain insight into the mode of dioxygen binding, the reaction of the O_2 analog NO with the diiron(II) centers of $R2_{red}$ has been investigated by spectroscopic methods. $R2_{red}$ reacts with NO to form an adduct with visible absorption features at 450 and 620 nm and Mössbauer parameters (δ = 0.75 mm/s, ΔE_Q = −2.13 and −1.73 mm/s) typical of those observed for $S = {}^3/_2$ {FeNO}^{7} complexes of other non-heme iron proteins. However, unlike other non-heme {FeNO}^{7} complexes, this adduct is EPR silent. Our Mössbauer studies show that each iron site of $R2_{red}$ binds one NO to form local $S = {}^3/_2$ {FeNO}^{7} centers which then couple antiferromagnetically ($J \approx 5$ cm^{-1}, $\mathcal{H} = J\mathbf{S}_1 \cdot \mathbf{S}_2$) to afford an {FeNO}$_2$ center (77% of total iron). This {FeNO}$_2$ center decomposes with a first-order rate constant of 0.013 min^{-1} to form $R2_{met}$, accompanied by the release of N_2O. These observations suggest that both iron(II) ions of the two diiron(II) centers of $R2_{red}$ have available sites for NO binding, in agreement with the crystallographic results on $R2_{red}$, and that the bound NO molecules are sufficiently close to each other to permit N−N bond formation to produce N_2O. These observations support the proposal that dioxygen binding may also involve both metal ions of the diiron(II) center to form a (μ-1,1-, or μ-1,2-peroxo)-diiron(III) center. This observed reactivity of $R2_{red}$ with NO may contribute to the *in vivo* inhibition of ribonucleotide reductase by NO.

The enzyme ribonucleotide reductase catalyzes the conversion of ribonucleotides to deoxyribonucleotides and provides a balance of each of the four deoxyribonucleotides needed for the first step of DNA biosynthesis (Reichard, 1993; Stubbe, 1990). Ribonucleotide reductase from *Escherichia coli* is composed of two proteins, R1 and R2. The R1 protein contains binding sites for substrates and allosteric effectors and provides the reducing equivalents for substrate reduction (Uhlin & Eklund, 1994). The R2 protein in the enzymatically active form, $R2_{ox}$,[1] contains a (μ-oxo)diiron(III) center and a stable tyrosine radical at position 122 (Tyr_{122}•) (Larsson & Sjöberg, 1986) positioned about 5 Å away from the nearest iron (Nordlund & Eklund, 1993; Nordlund et al., 1990). This radical initiates ribonucleotide reduction on the R1 protein, presumably by long-range transfer of this oxidizing equivalent (Nordlund & Eklund, 1993).

The formation of the essential Tyr_{122}• occurs during the reaction of dioxygen with the diiron(II) form of the protein, $R2_{red}$. Recent X-ray crystallographic studies of the S211A mutant protein (S211 is not a ligand to the diiron center) suggests that the diiron(II) centers of $R2_{red}$ consist of two ions, each ligated to one terminal histidine, one terminal carboxylate, and two bridging carboxylate ligands (Åberg, 1993). Some mechanisms that have been proposed for the Tyr_{122}• radical generation reaction (Ling et al., 1994b; Que, 1991) invoke a high valent iron intermediate, by analogy to those found in heme-containing enzymes (Dawson, 1988; Guengerich, 1991). A similar mechanism has also been proposed for the non-heme diiron center of methane monooxygenase (Lee et al., 1993). However, the recent characterization of intermediates in the radical generation mechanism of R2 has determined that the oxidizing equivalents do not necessarily reside on the iron centers but instead reside on a metal ligand or nearby protein residue (Bollinger et al., 1994a,b; Ravi et al., 1994). The differences observed in dioxygen reactivity at heme and non-heme iron centers provide an example of the variety of ways protein active sites are engineered to accommodate high valent states to accomplish similar chemistry.

The recently characterized intermediates in the radical generation reaction of R2 represent species subsequent to O−O bond cleavage; thus a peroxide intermediate has not yet been observed, which is presumably the first step of the mechanism (Ling et al., 1994b; Que, 1991). Support for this intermediate has been provided by the observation that H_2O_2 reacts with the radical-free (μ-oxo)diiron(III) form of the protein, $R2_{met}$, to generate Tyr_{122}• in a peroxide shunt pathway (Fontecave et al., 1990; Sahlin et al., 1990). Further support has recently arisen from the quantitative incorporation of ^{18}O

† This work was supported by grants from the National Science Foundation (MCB-9405723, L.Q.) and the National Institutes of Health (GM22701, E.M.) and by a National Institutes of Health predoctoral traineeship for C.J.H. (GM08277).

* To whom correspondence should be addressed.

‡ University of Minnesota.

§Carnegie Mellon University.

|| Current address: W. R. Grace & Co.-Conn., Washington Research Center, 7379 Route 32, Columbia, MD 21044.

⊗ Abstract published in *Advance ACS Abstracts,* August 15, 1995.

[1] Abbreviations: $R2_{ox}$, oxidized R2 protein of ribonucleotide reductase; $R2_{met}$, tyrosine radical-reduced diiron(III) form of the R2 protein of ribonucleotide reductase; $R2_{red}$, reduced R2 protein of ribonucleotide reductase; GC, gas chromatography; 3,4-PCD, protocatechuate 3,4-dioxygenase; 4,5-PCD, protocatechuate 4,5-dioxygenase; TPA, tris(2-pyridylmethyl)amine.

0006-2960/95/0434-11090$09.00/0

into the μ-oxo bridge of $R2_{ox}$ in the reaction of $R2_{red}$ with $^{18}O_2$ (Ling et al., 1994b). However, the peroxide coordination mode in this intermediate is not known. A number of proteins with dinuclear metal sites bind dioxygen to form a peroxide intermediate. Hemerythrin, a non-heme diiron protein involved in dioxygen transport, binds dioxygen to form a terminal, η^1 peroxide (Shiemke et al., 1986; Stenkamp, 1994). Hemocyanin, a dicopper dioxygen transport protein, binds dioxygen to form a μ-η^2:η^2 peroxide (Ling et al., 1994a; Magnus et al., 1994). Still other peroxide coordination modes have been observed by a number of diiron and dicopper model complexes (Paul et al., 1991; Dong et al., 1993; Feig & Lippard, 1994; Kitajima & Morooka, 1994; Kitajima et al., 1994). While it is not clear what will govern dioxygen reactivity, it is nevertheless important to gain insight into the dioxygen coordination mode and to relate it to protein function.

Valuable information regarding the coordination of dioxygen in the putative diiron peroxide intermediate in R2 may be provided by exploring the reaction of $R2_{red}$ with nitric oxide. Nitric oxide has been a valuable probe for the study of many non-heme iron proteins (Arciero et al., 1983; Chen et al., 1989; Orville & Lipscomb, 1993). Because of its similar structure and electronic properties, it can be used as an O_2 analog to study the mode of O_2 binding. For example, deoxyhemerythrin was shown to bind NO reversibly to one iron(II) site in a bent, end-on coordination mode, analogous to the O_2 binding mode in oxyhemerythrin (Nocek et al., 1988; Stenkamp, 1994). In addition, the unpaired electron of NO makes it a convenient spectroscopic probe because NO adducts formed by complexation with high spin Fe(II) are transformed into $S = {}^3/_2$ systems that exhibit characteristic EPR signals and Mössbauer spectra (Arciero et al., 1983; Bill et al., 1985; Chen et al., 1989; Brown et al., 1995); these NO complexes have been designated as $\{FeNO\}^7$ complexes (Enemark & Feltham, 1974). The rich chemistry precedented in the NO complexes of non-heme iron proteins has prompted an examination of the effect of NO on $R2_{red}$.

EXPERIMENTAL PROCEDURES

Purification of $R2_{ox}$ and ^{57}Fe-Enriched $R2_{ox}$. $R2_{ox}$ and ^{57}Fe-enriched $R2_{ox}$ were purified from *E. coli* strain N6405/pSPS2 (Salowe & Stubbe, 1986) according to published procedures (Lynch, 1989; Salowe, 1987). ^{57}Fe-enriched $R2_{ox}$ was prepared by adding a freshly made ^{57}Fe(II) solution buffered with 1.0 M HEPES/125 mM ascorbic acid (pH 5) to the cell suspension after treatment with lysozyme. A 15-min delay after lysozyme addition was found to be essential for achieving a high incorporation (nearly 100%) of ^{57}Fe into the R2 active sites. The purity of $R2_{ox}$ and ^{57}Fe-enriched $R2_{ox}$ was determined by absorption ratios of $A_{280}/A_{410} = 16$, $A_{410}/A_{405} = 1.19$, and $A_{280}/A_{370} = 13.5$ and the appearance of a single band on SDS−polyacrylamide gel electrophoresis. The protein concentration was determined by $\epsilon_{280} = 141$ mM^{-1} cm^{-1} (Lynch, 1989). After purification, $R2_{ox}$ and ^{57}Fe-enriched $R2_{ox}$ were treated identically.

Preparation of $R2_{met}$ and $R2_{red}$. $R2_{met}$ was prepared by adding hydroxyurea to $R2_{ox}$ (0.5 μL of 1.5 M hydroxyurea per mg) and incubating at room temperature for 15 min. Excess hydroxyurea was removed by dialysis for 8 h at 4 °C versus four changes of 50 mM HEPES buffer, pH 7.6, containing 5% glycerol (Barlow et al., 1983). The concentration of $R2_{met}$ was determined by $\epsilon_{280} = 130$ mM^{-1} cm^{-1}. To prepare $R2_{red}$, a solution of $R2_{met}$ and benzyl viologen in a molar ratio of 1:0.5 was degassed on ice by vacuum/argon cycles on a dual-manifold vacuum line equipped with a BASF Catalyst column to remove trace amounts of O_2 and was then treated with an anaerobic solution of sodium dithionite which immediately turned the protein solution purple due to the presence of reduced benzyl viologen. A dithionite/protein ratio of 4:1 was used for UV−vis, EPR, and Mössbauer experiments, and a molar ratio of 2:1 was used for GC quantitation experiments.

Preparation of $R2_{red}$ + NO Samples. $R2_{met}$ (0.38−2.0 mL of 0.10−0.50 mM) was reduced and incubated for 3 min in an anaerobic cuvette for UV−vis, EPR, and Mössbauer experiments or in a septum-capped 1-dram vial for GC quantitation experiments. Nitric oxide (in a fume hood) purified by passing through concentrated KOH was anaerobically delivered over the surface and bubbled directly into the protein sample for 1.0−1.5 min. The purple color of reduced benzyl viologen disappeared within approximately 10 s of NO addition, and the yellow-green color of the NO complex developed over the next 30−60 s in the presence of a large excess of NO. EPR and Mössbauer samples were prepared from the same solution by the anaerobic transfer of 300 μL to an EPR tube or Mössbauer cup and frozen in liquid N_2.

Physical Measurements. Optical spectra and kinetic data were recorded on a Beckman DU 640 spectrophotometer using 1.0 or 0.2 cm anaerobic cuvettes. EPR spectra were recorded on a Varian E109 spectrometer equipped with an Oxford ESR10 cryostat under the following conditions: temperature, 10 K; microwave frequency, 9.23 GHz; microwave power, 20 μW; modulation frequency, 100 kHz; and modulation amplitude, 10 G. EPR quantitations were carried out by double integration under nonsaturating conditions and comparison with a 0.474 mM Cu^{II}(EDTA) standard. Mössbauer spectra were recorded on either a strong-field or a weak-field spectrometer operating in a constant acceleration mode in a transmission geometry using Janis Research Inc. cryostats that allow for a variation in temperature from 1.5 to 300 K. One of the dewars housed a superconducting magnet that allowed for the application of magnetic fields up to 8 T parallel to the γ-radiation. The zero velocity of the Mössbauer spectra were referred to the centroid of the room-temperature spectrum of a metallic iron foil.

Kinetics of $\{FeNO\}_2$ Complex Decomposition. Samples of $R2_{red}$ + NO were prepared in an anaerobic cuvette (0.5 mL of 0.40 or 0.50 mM). Kinetic data were collected after the $\{FeNO\}_2$ complex began to decay by following the 620 nm band. The data were analyzed by two methods, the Kezdy−Swinbourne method [$P_t = P_\infty[1 - \exp(k\tau)] + P_{t+\tau}\exp(k\tau)$] and the Guggenheim method [$P_t - P_{t+\tau} = (P_o - P_\infty)[1 - \exp(-k\tau)]\exp(-kt)$] (Espenson, 1981), both of which are useful in determining the rate constant of a first-order reaction with no endpoint data. In both methods, the plotted data gave linear fits from which a rate constant was obtained.

N_2O Quantitation. The separation and detection of N_2O was performed on a Hewlett Packard 5890 series II gas chromatograph with a HP 3396 series II integrator using a Porpak Q column (6 ft) using a 20 mL/min flow rate at 30 °C with helium as the carrier gas. All samples were prepared in argon-flushed septum-capped 1-dram vials and contained

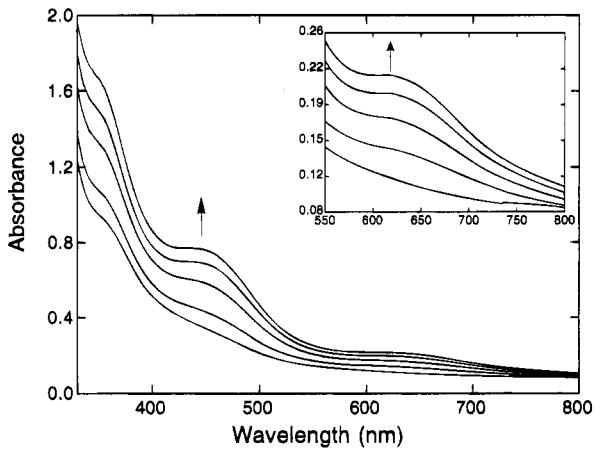

FIGURE 1: Optical spectra of 2.0 mL of 0.29 mM $R2_{red}$ (50 mM HEPES, pH 7.6, 5% glycerol) plus NO at 5, 10, 18, 24, and 30 min after initial NO exposure; the arrows indicate the reaction progress.

1.0 mL of 0.50 mM of the NO complex for sample vials or 1.0 mL of buffer for standard and control vials to correct for the volume and gas solubility differences. To each standard vial, 20, 30, 40, 60, or 80 μL of N_2O gas was added and a headspace aliquot (30 μL) was injected into the GC from which a standard curve of μmol of N_2O vs integration area was prepared. In protein sample vials, a headspace aliquot was injected 3−10 min after NO addition and again after 87−105 min. N_2O gas was detected at a retention time of 3.7−4.1 min as a well-resolved peak in all samples. The net amount of N_2O produced (μmol) during this time was determined after comparison with the standard curve. Control vials were treated identically to sample vials; each control vial containing dithionite was treated with NO and analyzed at the same two time points as the protein samples. Careful treatment of control vials was necessary to determine the background net N_2O production which was used to correct the net N_2O production in the protein samples.

RESULTS

Reaction of $R2_{red}$ with NO. The addition of nitric oxide to an anaerobic solution of $R2_{red}$ results in NO complexation. Complex formation is highly dependent upon the sample volume and protein concentration; an increase in either decreases the rate of formation, suggesting that the time required for NO dissolution is rate limiting. Because of this complication, the rate constant for the formation of this complex was not determined. NO complex formation can be observed for a range of volumes (0.38−2.0 mL) and protein concentrations (0.10−0.50 mM); however, the use of protein concentrations above 0.50 mM yields a mixture of $R2_{red}$ and the NO complex. To ensure complete reaction with $R2_{red}$, excess dissolved NO was always present in the protein solution.

The use of a large sample volume (2.0 mL of 0.29 mM $R2_{red}$) significantly slowed the reaction between $R2_{red}$ and NO to reveal the development of the optical spectrum from 5 to 30 min after initial NO exposure (Figure 1). The spectrum taken at 30 min shows maximal formation of this complex and exhibits absorption maxima at 350, 450, and 620 nm. The 450 and 620 nm bands of this yellow-green complex originate from an iron−nitrosyl complex. Similar absorption features, characteristic of iron−nitrosyl complexes, have been observed in a number of mononuclear and dinuclear non-heme iron−nitrosyl complexes in proteins and model complexes (Table 1). Using a variety of spectroscopic techniques, Solomon, Hodgson, and co-workers have recently proposed that the electronic structure of the $\{FeNO\}^7$ complexes is best described as high-spin iron(III) antiferromagnetically coupled to NO^- (Brown et al., 1995). These researchers have assigned the bands observed around 450 and 620 nm to NO^--to-Fe(III) charge transfer transitions. The 350 nm band observed in the $R2_{red}$ + NO sample does not originate from the iron−nitrosyl complex, since it is also present in anaerobic samples of $R2_{apo}$ to which NO has been added. This band has previously been assigned in isopenicillin N synthase-NO as arising from a nonspecific interaction of NO with proteins (Chen et al., 1989).

Samples of $R2_{red}$ + NO, for various protein concentrations, were frozen at different times after initial NO exposure (5−100 min) and studied by EPR spectroscopy. The spectra contained three distinct components that had, for different preparations, nearly identical shapes and relative concentrations (Figure 2). The major signal at g = 4.06, 3.98, and 2.01 belongs to an $S = {}^3/_2$ species indicative of an $\{FeNO\}^7$ complex (Table 1). Determination of the spin concentration of this signal for three independent $R2_{red}$ + NO preparations showed that it represents only 10−20% of the iron; these quantitations include a minority $S = {}^3/_2$ species discernible by the weaker signals in the wings of the $g \approx 4$ feature. A second signal, with a spin concentration of ~1−2% of the iron, is observed at g = 2.02 and 2.03. This signal showed slight broadening when ^{56}Fe was replaced by ^{57}Fe, suggesting that it results from an iron-containing complex. Such signals are commonly observed for $[Fe(NO)_2(SR)_2]$ complexes (Kennedy et al., 1993), and the signal observed here may

Table 1: Spectroscopic Properties of Non-Heme $\{FeNO\}^7$ Complexes

sample	λ_{max} (nm) ϵ (cm^{-1} M^{-1})	δ (mm/s)	ΔE_Q (mm/s)	g values	A_{iso}[a] (MHz)	reference
$\{FeNO\}_2$ complex of R2	450 (760)[b] 620 (220)[b]	0.75	−2.13		−31.5	this work
		0.75	−1.73		−34.2	
$\{FeNO\}^7$ complex of R2	450 (760)[b] 620 (220)[b]	0.70	−1.7	4.06, 3.98, 2.01	−34.7	this work
isopenicillin N synthase-NO	430 (800) 600	0.75	−1.0	4.09, 3.95, 2.00	−37.0	Chen et al. (1989)
Fe(EDTA)NO	440 (550) 660 (110)	0.66	−1.67	4.1, 3.9, 2.0	−35.7	Arciero et al. (1983), Brown et al. (1995)
4,5-PCD-NO		0.66	−1.67	4.09, 3.91, 2.0	−32.0	Arciero et al. (1983)
putidamonooxin-NO		0.68	−1.4	4.0, 4.0, 2.0	−32	Bill et al. (1985)
reduced 3,4-PCD-NO	430 (1870) 650			4.34, 3.69, 1.98		Orville and Lipscomb (1993)
soybean lipoxygenase-NO				4.0, 4.0, 2.0		Nelson (1987)
deoxyhemerythrin-NO	408 (1200) 600 (500)	0.68	0.61	2.77, 1.84, 1.84		Nocek et al. (1988)
($S = {}^1/_2$)	500 (700)	1.21	2.65			

[a] Isotropic part of ^{57}Fe magnetic hyperfine tensor; $A_{iso} = (A_x + A_y + A_z)/3$. [b] Both $\{FeNO\}_2$ and $\{FeNO\}^7$ are assumed to contribute with identical ϵ to the optical spectrum which is scaled to reflect 90% of the iron in the sample.

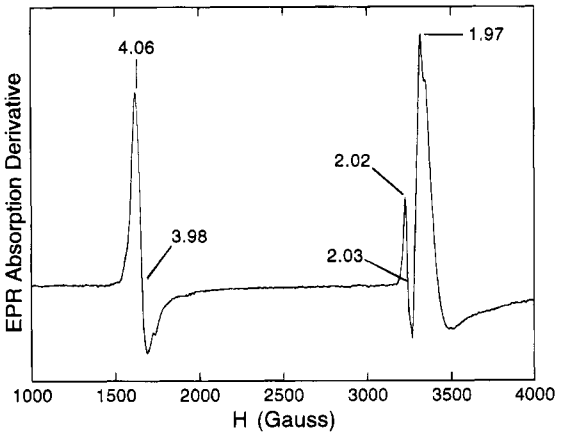

FIGURE 2: X-band EPR spectrum of 0.29 mM $R2_{red}$ (50 mM HEPES, pH 7.6, 5% glycerol) plus NO frozen 100 min after initial NO exposure. Instrumental conditions: temperature, 10 K; microwave frequency, 9.23 GHz; microwave power, 0.02 mW; modulation frequency, 100 kHz; and modulation amplitude, 10 G.

arise from a similar complex with any of the 10 available solvent-accessible cysteine residues of R2 (Nordlund & Eklund, 1993). A third signal is observed at $g \approx 1.97$. This feature was also present in control samples containing buffer + NO or $R2_{apo}$ + NO and is attributed to NO in solution. Finally, studies of $R2_{red}$ + NO in a bimodal cavity did not reveal any integer-spin EPR signal. Thus, our studies show that only a small fraction of the iron in $R2_{red}$ + NO samples resides in EPR-active complexes; moreover, none of the signals observed represents a dinuclear center.

In order to investigate the EPR-silent species, Mössbauer samples of $R2_{red}$ + NO were obtained under conditions to ensure maximum NO complex formation by following the time course of the optical spectra. The 4.2 K Mössbauer spectrum of a representative sample, frozen 12 min after NO exposure, is shown in Figure 3. The spectrum contains the contribution of three distinct iron complexes (Table 2). The contribution of the $S = {}^3/_2$ $\{FeNO\}^7$ complex is readily recognized by the presence of a component that exhibits magnetic hyperfine structure. This component has spectral parameters very similar to those reported for other $\{FeNO\}^7$ complexes (Table 1); thus, its Mössbauer spectrum could be readily computed from a suitable $S = {}^3/_2$ spin Hamiltonian (see below); a theoretical curve for this species, scaled to represent 13% of total iron, is drawn through the data of Figure 3. A second species, accounting for 77% of the iron, gives rise to the major doublet in the central portion of the spectrum. We will argue below that it belongs to an EPR-silent dinuclear center which has one NO bound to each iron site. A third, minor component exhibiting a quadrupole doublet with $\Delta E_Q \approx 1.4$ mm/s and $\delta \approx 0.07$ mm/s appears also in the central portion of the spectrum. This doublet seems to belong to a diamagnetic iron environment of unknown nature; its contribution, representing 10% of the iron, is shown above the data in Figure 3. Five independent preparations of $R2_{red}$ + NO showed the same collection of species with similar relative concentrations. A control sample, made by anaerobic addition of NO to $R2_{met}$, exhibited only the two quadrupole doublets (data not shown) characteristic of the native diiron(III) center of $R2_{met}$, showing that NO does not bind to the diiron(III) center.

The Mössbauer spectrum of the diiron(III) center of native R2 consists of two quadrupole doublets with $\delta_1 = 0.45$ mm/s and $\delta_2 = 0.55$ mm/s, while that of $R2_{red}$ corresponds to two nearly identical high-spin iron(II) sites with $\delta_1 \approx \delta_2 = 1.25$ mm/s (Lynch et al., 1989). In contrast, $\{FeNO\}^7$ complexes have δ values ranging from 0.66 to 0.75 mm/s (Table 1); the $\{FeNO\}^7$ complex observed here has a similar shift, namely, $\delta \approx 0.70$ mm/s. A similar shift, $\delta = 0.75$ mm/s, is also observed for the major doublet in the spectrum of Figure 3. A detailed analysis of our data set suggests that this doublet actually consists of two components with $\delta_1 \approx \delta_2 \approx 0.75$ mm/s and $\Delta E_Q(1) = -1.73$ mm/s and $\Delta E_Q(2) = -2.13$ mm/s. Since this species produces quadrupole doublets at 4.2 K, rather than magnetically split spectra, the complex must have integer electronic spin. Taken together, our data suggest that we are dealing with a diiron center containing two exchange-coupled $S = {}^3/_2$ $\{FeNO\}^7$ sites in an $\{FeNO\}_2$ complex. This interpretation is supported by the observation that the optical spectra of $R2_{red}$ + NO exhibit bands characteristic of $\{FeNO\}^7$ complexes (Table 1). If all of the absorption were attributed to the minority $\{FeNO\}^7$ complex, this species would have an $\epsilon \approx 6000$ M^{-1} cm^{-1} at 450 nm, substantially larger than those reported for other iron−nitrosyl complexes. However, if we assume that the majority species is a dinuclear $\{FeNO\}_2$ complex for which each iron site produces an $\{FeNO\}^7$-type optical spectrum, we would obtain a reasonable $\epsilon = 760$ M^{-1} cm^{-1} per iron, in agreement with values from other iron−nitrosyl complexes (Table 1).

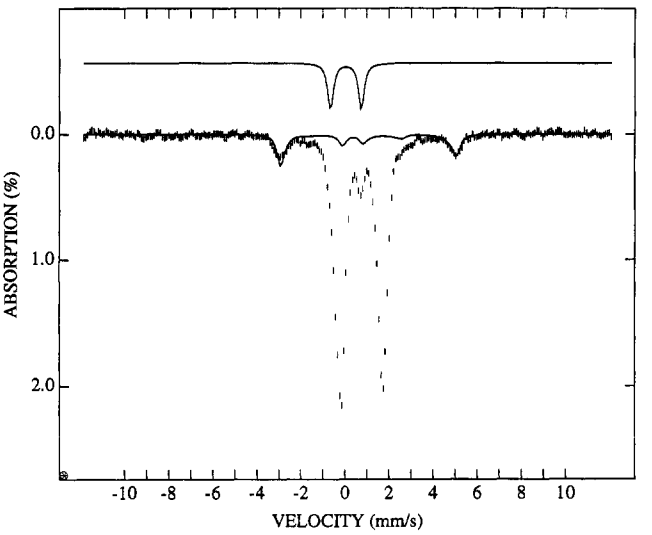

FIGURE 3: Mössbauer spectrum of 0.48 mM ^{57}Fe-enriched $R2_{red}$ (50 mM HEPES, pH 7.6, 5% glycerol) + NO frozen 12 min after exposure to NO. The spectrum was recorded at 4.2 K in a parallel field of 0.05 T. The solid line drawn through the data is a theoretical curve representing the mononuclear $S = {}^3/_2$ $\{FeNO\}^7$ complex (13% of Fe). The curve was generated from eqs 1−3 using $D = 9$ cm^{-1}, $E/D = 0.02$, $A = -34.2$, -31.5, and -38.4 MHz, $\Delta E_Q = -1.7$ mm/s, $\eta = 0$, and $\delta = 0.70$ mm/s. The doublet shown above the data indicates the contribution (10% of Fe) of the unidentified species with $\Delta E_Q = 1.4$ mm/s and $\delta = 0.04$ mm/s.

Table 2: Mössbauer Parameters and Assignments for Reduced R2 + NO Samples

	fraction (%)				
assignment	12 min	100 min	300 min	δ (mm/s)	ΔE_Q (mm/s)
$\{FeNO\}_2$	77	30	22	0.75, 0.75	−2.13, −1.73
$\{FeNO\}^7$	13	13	13	0.70	−1.7
$R2_{met}$	0	42	47	0.55, 0.45	−1.62, −2.44
unknown	10	14	18	0.07	1.4

The $\{FeNO\}^7$ complex observed here to give rise to an $S = {}^3/_2$ EPR signal cannot result from a diiron center. If one NO would bind to one iron of $R2_{red}$, the resulting $S = {}^3/_2$ site would strongly interact with the nearby iron(II), either by exchange interactions as observed for deoxyhemerythrin-NO (Nocek et al., 1988) or by strong dipolar interactions that would be recognized with EPR or low-field Mössbauer spectroscopy. Our data are incompatible with either case. Moreover, the high temperature Mössbauer spectra of the sample of Figure 3 did not indicate the presence of any iron(II). This suggests that an $\{FeNO\}^7$ complex is formed when NO binds to adventitiously bound iron(II). Since our R2 samples did not contain adventitiously bound iron prior to treatment with NO, some destruction of the diiron center must occur during incubation with NO.

The Mössbauer spectra of mononuclear $S = {}^3/_2$ $\{FeNO\}^7$ complexes can be analyzed with the $S = {}^3/_2$ spin Hamiltonian:

$$\mathcal{H} = \mathcal{H}_e + \mathcal{H}_n \quad (1)$$

with

$$\mathcal{H}_e = \mathbf{S}\cdot\mathbf{D}\cdot\mathbf{S} + g_0\beta\mathbf{S}\cdot\mathbf{H} \quad (2)$$

and

$$\mathcal{H}_n = \mathbf{S}\cdot\mathbf{A}\cdot\mathbf{I} + \mathbf{I}\cdot\mathbf{P}\cdot\mathbf{I} - g_n\beta\mathbf{H}\cdot\mathbf{I} \quad (3)$$

where all symbols have their conventional meanings and where $g_0 = 2.0$. Mössbauer and EPR studies of a variety of $\{FeNO\}^7$ complexes have revealed a striking similarity of the fine structure and hyperfine structure parameters ($D \approx 10-14$ cm^{-1}, $E/D \approx 0$, $A_{iso} \approx -34$ MHz). The $\{FeNO\}^7$ minority species observed here has parameters (see caption of Figure 3) very similar to those reported for other NO complexes (Arciero et al., 1983; Bill et al., 1985; Chen et al., 1989; Nocek et al., 1988). We have used this parameter set to simulate the high-field spectra of the $\{FeNO\}^7$ minority species; the spectra displayed in Figure 4 were obtained by subtracting its simulated contribution (13%) from the raw data.

As pointed out above, the Mössbauer spectra of the $\{FeNO\}_2$ species suggests an electronic system consisting of two exchange coupled $S = {}^3/_2$ sites. The electronic features of this coupled system can be explored with the Hamiltonian:

$$\mathcal{H} = J\mathbf{S}_1\cdot\mathbf{S}_2 + \mathcal{H}_e(1) + \mathcal{H}_e(2) \quad (4)$$

where $S_1 = S_2 = {}^3/_2$ and the $\mathcal{H}_e(i)$ is given by eq 2. Because of the large D values of the mononuclear NO complexes, the electronic properties of the coupled system will be strongly dependent on the zero-field splitting terms. We have investigated the spin expectation values resulting from eq 4, allowing the D tensors of the two sites to be rotated relative to each other. These studies have shown that the magnetic features of the spectra of Figure 4 cannot be explained by assuming ferromagnetic coupling ($J < 0$). Thus, for any $J < 0$, eq 4 would predict, contrary to the experimental observations, the observation of strong magnetic hyperfine interactions in an applied field of 2 T. For antiferromagnetic coupling, two regimes can be distinguished. For $J > D$, the ground state would essentially be a pure $S = 0$ level that would yield, at 4.2 K, Mössbauer spectra characteristic of a diamagnetic compound. However, the 8.0 T spectrum displays substantial paramagnetic hyperfine structure; therefore, the case $J > D$ can be excluded. This suggests that $0 \leq J \leq 15$ cm^{-1}. Keeping all local parameters of the two sites to within 20% of those observed for mononuclear $\{FeNO\}^7$ species, we have performed spectral simulations allowing J and the relative orientations of the D tensors to vary. The best simulations, shown in Figure 4, were obtained for $J = 5$ cm^{-1} for the case where the z axes of both D tensors, i.e., the axes of near axial local symmetry, are tilted 30° relative to each other. All $\{FeNO\}^7$ complexes studied thus far have $E/D \approx 0$, suggesting that the NO ligand imposes nearly axial symmetry on the $S = {}^3/_2$ system. It is thus not surprising to find that the individual D tensors of the $\{FeNO\}_2$ complex should have different principal axis systems.

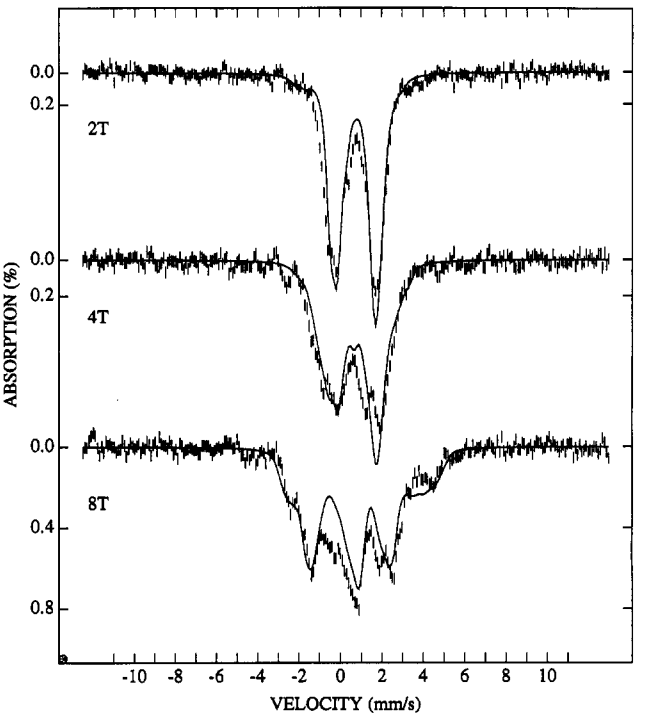

FIGURE 4: 4.2 K Mössbauer spectra of $R2_{red}$ + NO (same sample as that of Figure 3). Spectra were recorded in parallel applied fields as indicated. The spectra were prepared from the raw data by subtracting the theoretical spectra (13% of total absorption) of the monomeric $S = {}^3/_2$ $\{FeNO\}^7$ complex. The data shown still contain the 10% contribution of the unknown species with $\Delta E_Q \approx 1.4$ mm/s and $\delta \approx 0.07$ mm/s. The theoretical curves are spectral simulations for a system consisting of two coupled $S = {}^3/_2$ species with $J = 5$ cm^{-1}, $D_1 = D_2 = 14$ cm^{-1}, $(E/D)_1 = (E/D)_2 = 0.02$, isotropic $A_1 = -31.5$ MHz and $A_2 = -35$ MHz, $\Delta E_Q(1) = -1.7$ mm/s, $\Delta E_Q(2) = -2.1$ mm/s, $\eta_1 = \eta_2 = 0$, and $\delta_1 = \delta_2 = 0.75$ mm/s. Moreover, the z axes of the two D tensors are tilted by 30° relative to each other. The theoretical curves are plotted to represent the fraction of $\{FeNO\}_2$, i.e., 87% of the data shown.

Reactivity of the $\{FeNO\}_2$ Complex. Changes were observed in both the optical and Mössbauer spectra of $R2_{red}$ + NO samples upon standing. However, no significant change was observed in its EPR spectrum, indicating that the mononuclear $\{FeNO\}^7$ component is unaffected. Analysis of the optical spectra taken between 40 and 100 min after initial NO exposure of $R2_{red}$ to NO shows a slow conversion to the final spectrum (Figure 5). This conversion is evidenced by the appearance of a new band at 370 nm and a decrease in both the 450 and 620 nm bands with an

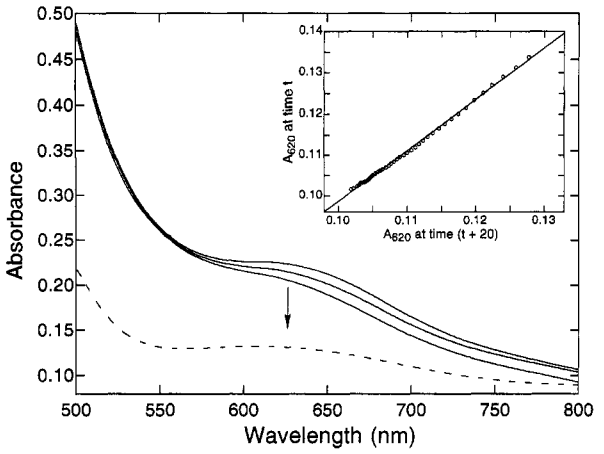

FIGURE 5: Optical spectra of 2.0 mL of 0.29 mM $R2_{red}$ (50 mM HEPES, pH 7.6, 5% glycerol) plus NO at 40, 50, and 100 min after initial NO exposure; the arrow indicates the reaction progress. For comparison, the dashed line shows the spectrum of $R2_{met}$ at the same concentration. The inset shows a Kezdy−Swinbourne plot of kinetic data from 20 to 230 min after exposure of 0.5 mL of 0.40 mM $R2_{red}$ (50 mM HEPES, pH 7.6, 5% glycerol) to NO.

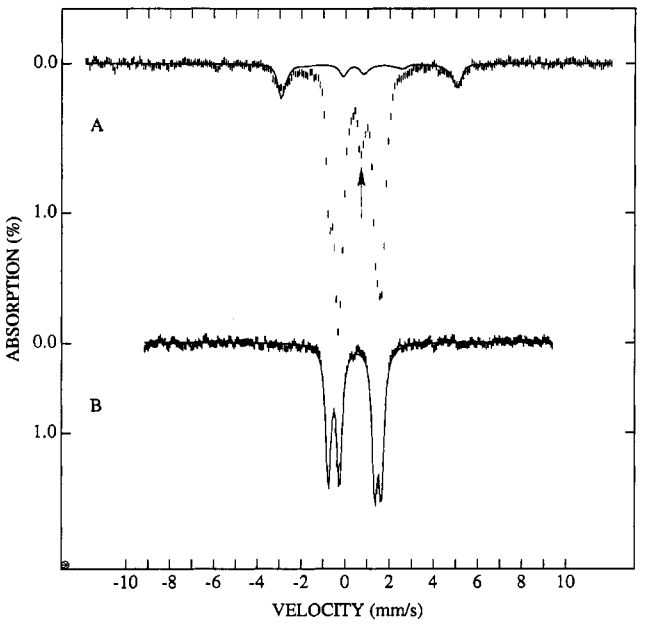

FIGURE 6: (A) 4.2 K Mössbauer spectrum of 0.48 mM ^{57}Fe-enriched $R2_{red}$ (50 mM HEPES, pH 7.6, 5% glycerol) + NO frozen 100 min after exposure to NO. The solid line drawn through the spectrum represents the contribution of the $\{FeNO\}^7$ complex scaled to 13% of the total absorption. The arrow indicates the high energy line of the quadrupole doublet of the unidentified species. (B) 4.2 K Mössbauer spectrum of $R2_{met}$.

isosbestic point at 440 nm, due to the decay of the $\{FeNO\}_2$ complex. The spectral evolution suggests that $\{FeNO\}_2$ converts to a new species that resembles $R2_{met}$.

The changes observed in the optical spectra are also evident in the Mössbauer spectra. Figure 6A shows a 4.2 K Mössbauer spectrum of a $R2_{red}$ + NO sample frozen 100 min after exposure to NO. The spectrum shows that 13% of the iron in the sample belongs to the $S = {}^3/_2$ $\{FeNO\}^7$ complex, which remains unchanged from the original sample; its contribution is outlined by the theoretical curve drawn through the data. The spectrum exhibits additional contributions from the $\{FeNO\}_2$ complex (30%) and from $R2_{met}$ (42%) (Table 2). The presence of the latter is indicated by the shoulder at the low-energy band of the doublet in the central portion of the spectrum; for comparison, the spectrum of $R2_{met}$ is shown in Figure 6B. Finally, the spectrum contains 14% of the unidentified species with $\Delta E_Q \approx 1.4$ mm/s and $\delta \approx 0.07$ mm/s; the high-energy line of this doublet is marked by the arrow. A second sample gave essentially identical results. Analysis of a sample of $R2_{red}$ + NO frozen 300 min after exposure to NO revealed a composition very similar to that of the 100 min samples; the amount of $R2_{met}$ had slightly increased to 47% of the sample (Table 2).

The experiments just described show that $R2_{met}$ is formed at the expense of the $\{FeNO\}_2$ complex. To further characterize this conversion, kinetic data were obtained by monitoring the optical absorbance at 620 nm from 20 to 230 min. These data, analyzed by the Kezdy−Swinbourne (Figure 5, inset) and Guggenheim methods (Espenson, 1981), indicated a first-order decomposition process and showed linear fits for five half-lives with a first-order rate constant of 0.013 ± 0.001 min^{-1}. As expected, changing the protein concentration did not affect the rate constant derived from the kinetic analyses.

The conversion of $\{FeNO\}_2$ to $R2_{met}$ raises a question as to the fate of the bound NO. One mechanistic possibility is that the oxo bridge in the formed $R2_{met}$ derived from bound NO accompanied by N_2O release. To detect N_2O, the headspace gas was analyzed by gas chromatography at maximum NO complex concentration (~6 min) and at approximately 100 min after NO addition. The net N_2O detected in all samples was due to a combination of that produced by the conversion reaction and by background N_2O. Control samples showed that background N_2O was present in all samples due to a combination of contaminating N_2O gas in the NO added to the sample and N_2O gas produced by the reaction of NO with trace amounts of dithionite not consumed by the reduction of $R2_{met}$. To correct for this, the background net N_2O production (0.47 μmol) was subtracted from the net N_2O production (0.79 μmol). The corrected amount of N_2O detected in three independent reactions was 0.35, 0.33, and 0.30 equiv per diiron center. Because of the high background level of N_2O, the error in quantitation is estimated to be ±0.06. These values thus correspond to the amount of $R2_{met}$ formed (0.4 equiv) in the decomposition of the $\{FeNO\}_2$ complex detected in the Mössbauer spectrum (Table 2).

DISCUSSION

Nitric oxide reacts with the diiron centers of $R2_{red}$ to form a mixture of three species. The majority species is an $\{FeNO\}_2$ complex (77%) which results from the binding of one NO molecule to each iron(II) of $R2_{red}$ to form a weakly coupled antiferromagnetic pair of $\{FeNO\}^7$ centers ($J \approx 5$ cm^{-1}; $\mathcal{H} = J\mathbf{S}_1\cdot\mathbf{S}_2$). The second species is an $\{FeNO\}^7$ complex (13%) formed when NO binds to adventitious iron(II), while the third species (10%) is of unknown origin. These assignments are primarily based on Mössbauer spectroscopy and supported by optical and EPR evidence; the two nitrosyl complexes observed have spectral properties similar to those of other non-heme mononuclear and dinuclear iron−nitrosyl complexes (Table 1).

The weak antiferromagnetic interaction between the $\{FeNO\}^7$ centers of the $\{FeNO\}_2$ complex suggests that the

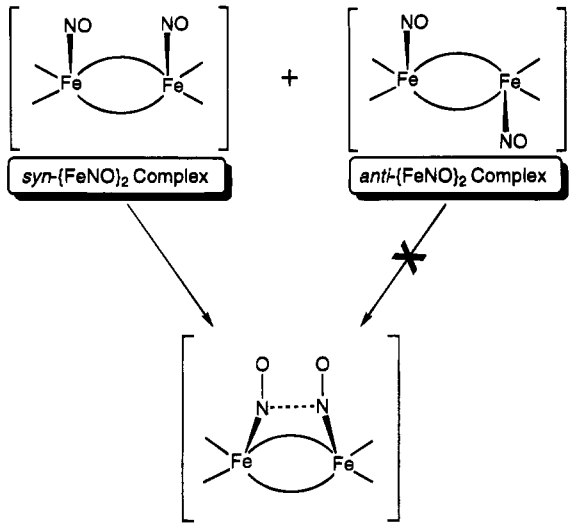

FIGURE 7: Two possible ways for NO to coordinate to $R2_{red}$ to form the $\{FeNO\}_2$ complex. N−N bond formation would occur only with the *syn*-bound form as shown.

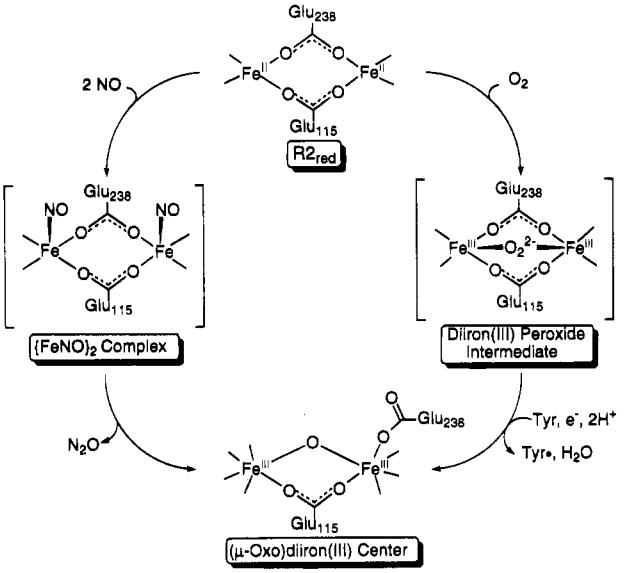

FIGURE 8: Proposed partial reaction mechanisms for the reactions of NO and O_2 with $R2_{red}$.

coupling interaction is unlikely to be mediated by hydroxo or oxo bridges. The absence of information on dinuclear $\{FeNO\}^7$ complexes forces us to make comparisons using the larger database of diiron(III) and diiron(II) complexes (Kurtz, 1990; Que & True, 1990). Oxo bridges are only observed in diiron(III) complexes and lead to coupling constants above 200 cm^{-1}, while hydroxo-bridged diiron(III) and diiron(II) complexes have coupling constants of 25−35 cm^{-1} (Kurtz, 1990; Que & True, 1990). On the other hand, (μ-aqua)diiron(II) complexes with two supporting carboxylate bridges have been synthesized and found to exhibit weak antiferromagnetic coupling [see footnote 7 in Hagen and Lachicotte (1992)]. The presence of this core structure may account for the observed coupling in the $\{FeNO\}_2$ complex. Weak antiferromagnetic coupling (2 cm^{-1}) has also been observed for $[Fe_2(\mu\text{-}O_2CCH_3)_2(TPA)_2](BPh_4)_2$ (Ménage et al., 1992), a complex which shares the same bis(μ-carboxylato)diiron(II) core structure as $R2_{red}$ (Åberg, 1993). Thus, the $\{FeNO\}_2$ complex could arise from the binding of NO to each of the coordinatively unsaturated iron(II) centers of $R2_{red}$ with the core remaining intact (Figure 7). This is also consistent with the observation that two azide ions can bind to the diiron(II) center at high azide concentrations (Elgren et al., 1993).

NO has been very useful as an O_2 analog to probe the interaction of dioxygen with non-heme iron(II) centers (Arciero et al., 1983; Chen et al., 1989; Orville & Lipscomb, 1993). The fact that NO reacts with $R2_{red}$ to afford an $\{FeNO\}_2$ complex can shed light on the nature of the putative peroxide intermediate in the oxidation of $R2_{red}$ to $R2_{ox}$. It is known that each diiron(II) center of $R2_{red}$ reacts with one dioxygen molecule (Elgren et al., 1991). This initial interaction of dioxygen with $R2_{red}$ has been proposed to result in the transfer of two electrons from the diiron(II) center to O_2 forming a diiron(III) peroxide intermediate (Fontecave et al., 1990; Ling et al., 1994a; Sahlin et al., 1990). However, this intermediate has not been observed in rapid kinetics studies (Bollinger et al., 1994a,b; Ravi et al., 1994), so the coordination mode of the peroxide in this putative intermediate is not known. The possibilities include terminal η^1-peroxo, μ-η^2:η^2-peroxo, μ-1,1-peroxo, and μ-1,2-peroxo coordination. When NO is used as a probe for O_2 binding to deoxyhemerythrin, a mono-NO adduct is formed due to the availability of only one exogenous ligand binding site (Stenkamp, 1994). This adduct is described as $[Fe^{II}Fe^{III}\text{-}NO^-]$ modeling the putative $[Fe^{II}Fe^{III}\text{-}O_2^-]$ intermediate en route to oxyhemerythrin (Nocek et al., 1988). The observation of coupled $\{FeNO\}^7$ centers in the $\{FeNO\}_2$ complex of R2 demonstrates that NO can access both iron(II) ions of the diiron(II) center and suggests that the bis(μ-carboxylato)-diiron core remains intact (Figure 8). The spectroscopic data cannot support a diiron structure with one NO bridging the two iron ions because such a moiety would not have a diamagnetic ground state. In the $\{FeNO\}_2$ complex, each NO molecule accepts an electron from the diiron(II) center, modeling the proposed two-electron reduction of O_2 to peroxide in the initial step of the oxidation of $R2_{red}$. We thus favor a μ-1,1- or a μ-1,2-peroxo mode for the proposed O_2 adduct of $R2_{red}$.

The notion of a bridged peroxide intermediate is further supported by the observed conversion of the $\{FeNO\}_2$ complex to $R2_{met}$ and N_2O. This conversion is indicated by the appearance of a new species in the Mössbauer spectrum at the expense of the $\{FeNO\}_2$ complex. The new species has an absorption band at 370 nm and Mössbauer parameters that are consistent with its assignment to $R2_{met}$. Analysis of the kinetics of conversion reveals that this decomposition is a first-order reaction with a rate constant of 0.013 min^{-1}. Furthermore, GC analysis of the reaction vial headspace gas shows that N_2O is produced during this conversion in amounts nearly equimolar with the amount of $R2_{met}$ formed. The formation of N_2O requires N−N bond formation from presumably proximally bound NO molecules. For the $\{FeNO\}_2$ complex, this would be best accomplished with a *syn*-bound species as shown in Figure 7. The same available coordination sites that allow a *syn*-bound $\{FeNO\}_2$ complex to form would also permit a bridged peroxide intermediate to form. The observation that a significant portion (22%) of the $\{FeNO\}_2$ complex remains after 300 min suggests that there is a minority population of $\{FeNO\}_2$ that cannot convert to $R2_{met}$ and N_2O. This minor subset may consist of molecules with the two NO's bound *anti* with respect to each other (Figure 7), so that N−N bond formation cannot occur.

This study is the first example of N_2O formation from the reaction of NO with iron(II) in non-heme iron proteins. Recent spectroscopic studies conclude that the binding of NO to an Fe(II) center results in the transfer of electron density from the Fe(II) to the NO forming an Fe(III)-NO^- species (Brown et al., 1995). The two NO^- moieties of the $\{FeNO\}_2$ complex can then couple to afford an equivalent of N_2O and an oxide ion which resides as a bridge between the iron(III) ions of $R2_{met}$. This reaction can be related to the reductive coupling of two NO molecules that is known to occur in solution ($2H^+ + 2e^- + 2NO \rightarrow N_2O + H_2O$) (Bottomley, 1989). Deoxyhemerythrin-NO does not undergo similar decomposition to produce N_2O presumably because only one molecule of NO is present in the active site (Nocek et al., 1988), but it is possible that other dinuclear non-heme iron proteins that can bind 2 equiv of NO can also carry out the conversion of NO to N_2O. It should be noted that N_2O formation has precedence with other proteins and model complexes. For example, the reduced forms of the dicopper protein hemocyanin (Verplaaetse et al., 1979) and the copper−heme protein cytochrome *c* oxidase (Brudvig et al., 1980) each react with two NO molecules forming dinitrosyl intermediates which decompose to yield N_2O and the oxidized proteins. N_2O formation has also been demonstrated in the reactions of copper model complexes with NO (Paul & Karlin, 1991). Each copper center reacts with an equivalent of NO to form an unstable intermediate, which decomposes to form a (μ-oxo)dicopper(II) complex accompanied by the release of N_2O. These results, and the observed decomposition of the R2 $\{FeNO\}_2$ species, suggest that the formation of the thermodynamically stable oxo-bridged dimetal center may promote N_2O formation. That this is also the driving force in the reaction of $R2_{red}$ with O_2 strengthens the argument that NO serves as a good probe of the dioxygen binding site of non-heme iron proteins. The slow conversion of $\{FeNO\}_2$ to N_2O may be due to rate-limiting N−N bond formation. The diiron center understandably may not be as efficient for carrying out such a coupling reaction, since this step is not encountered in the corresponding O_2 reaction.

A mechanism consistent with the results obtained from the majority of the sample in the reaction of NO with $R2_{red}$ is shown in Figure 8 with the proposed reaction of O_2 with $R2_{red}$. In this mechanism, the $\{FeNO\}_2$ complex is an intermediate that parallels the proposed bridging diiron(III) peroxide intermediate of the radical generating reaction. The bridging peroxide intermediate contrasts the η^1-hydroperoxo adduct that forms in the reaction of O_2 with deoxyhemerythrin. This difference in peroxide coordination may play a role in the subsequent reactivity of these intermediates and therefore in overall protein function. To what extent the peroxide coordination mode influences its subsequent reactivity is not presently known and must await information from the investigations of peroxide intermediates of other diiron proteins and model complexes. Both the $\{FeNO\}_2$ and peroxide intermediates of R2 spontaneously convert to the (μ-oxo)diiron(III) center; the NO reaction releases N_2O in this process while the O_2 reaction oxidizes Tyr_{122}. Thus, the reaction of $R2_{red}$ with NO can be viewed as a two-electron analog for the four-electron dioxygen reaction. Although the (μ-oxo)diiron(III) center is formed in both reactions, only the dioxygen reaction has the additional oxidizing equivalents to generate the essential $Tyr_{122}^{\bullet}$.

The observed reactivity of $R2_{red}$ with NO may contribute to the *in vivo* inhibition of ribonucleotide reductase by NO. The body's immune system has macrophages that deliver large amounts of NO, via NO synthase, to nearby tumor cells where it can affect several metalloenzymes, one of which is ribonucleotide reductase. It is known that stimulated macrophages produce enough NO to inhibit the enzyme so that the conversion of ribonucleotides into deoxyribonucleotides stops (Feldman et al., 1993). Previously, it has been shown that NO destroys the $Tyr_{122}^{\bullet}$ in tumor cells and in purified bacterial or mammalian R2 proteins, thereby inhibiting ribonucleotide reductase activity (Lepoivre et al., 1991, 1992, 1994). It has been proposed that this inhibition results from $Tyr_{122}^{\bullet}$ quenching by NO. However, the reaction of NO with the diiron(II) center may provide another mechanism for the inhibition of ribonucleotide reductase. The regeneration of active R2 requires reduction to its $R2_{red}$ form and subsequent reaction with O_2. NO can oxidize $R2_{red}$ to form $R2_{met}$ without forming the catalytically essential $Tyr_{122}^{\bullet}$; thus the resulting R1R2 holoenzyme complex will not be capable of reducing the substrate ribonucleotides.

ACKNOWLEDGMENT

We thank Professor J. Stubbe for providing *E. coli* strain N6405/pSPS2, Professor John D. Lipscomb for the use of the EPR spectrometer, and Professor William B. Tolman for the use of the gas chromatograph and N_2O gas. We thank Professor Michael P. Hendrich for valuable discussions about EPR spectroscopy. We also thank Christy E. Ruggiero and Susan M. Carrier for assistance in N_2O quantitation and kinetic data interpretation.

REFERENCES

Åberg, A. (1993) Ph.D. Thesis, Stockholm University.
Arciero, D. M., Lipscomb, J. D., Huynh, B. H., Kent, T. A., & Münck, E. (1983) *J. Biol. Chem. 258*, 14981−14991.
Barlow, T., Eliasson, R., Platz, A., Reichard, P., & Sjöberg, B.-M. (1983) *Proc. Natl. Acad. Sci. U.S.A. 80*, 1492−1495.
Bill, E., Bernhardt, F.-H., Trautwein, A. X., & Winkler, H. (1985) *Eur. J. Biochem. 147*, 177−182.
Bollinger, J. M., Jr., Tong, W. H., Ravi, N., Huynh, B. H., Edmondson, D. E., & Stubbe, J. (1994a) *J. Am. Chem. Soc. 116*, 8015−8023.
Bollinger, J. M., Jr., Tong, W. H., Ravi, N., Huynh, B. H., Edmondson, D. E., & Stubbe, J. (1994b) *J. Am. Chem. Soc. 116*, 8024−8032.
Bottomley, F. (1989) *Reactions of Coordinated Ligands*, Plenum Press, New York.
Brown, C. A., Pavlosky, M. A., Westre, T. E., Zhang, Y., Hedman, B., Hodgson, K. O., & Solomon, E. I. (1995) *J. Am. Chem. Soc. 117*, 715−732.
Brudvig, G. W., Stevens, T. H., & Chan, S. I. (1980) *Biochemistry 19*, 5275−5285.
Chen, V. J., Orville, A. M., Harpel, M. R., Frolik, C. A., Surerus, K. K., Münck, E., & Lipscomb, J. D. (1989) *J. Biol. Chem. 264*, 21677−21681.
Dawson, J. H. (1988) *Science 240*, 433−439.
Dong, Y., Ménage, S., Brennan, B. A., Elgren, T. E., Jang, H. G., Pearce, L. L., & Que, L., Jr. (1993) *J. Am. Chem. Soc. 115*, 1851−1859.
Elgren, T. E., Lynch, J. B., Juarez-Garcia, C., Münck, E., Sjöberg, B.-M., & Que, L., Jr. (1991) *J. Biol. Chem. 266*, 19265−19268.
Elgren, T. E., Hendrich, M. P., & Que, L., Jr. (1993) *J. Am. Chem. Soc. 115*, 9291−9292.
Enemark, J. H., & Feltham, R. D. (1974) *Coord. Chem. Rev. 13*, 339−406.
Espenson, J. H. (1981) *Chemical Kinetics and Reaction Mechanisms*, McGraw-Hill, Inc., New York.

Feig, A. L., & Lippard, S. J. (1994) *Chem. Rev. 94*, 759−805.
Feldman, P. L., Griffity, O. W., & Stuehr, D. J. (1993) *Chem. Eng. News 71*, 26−38.
Fontecave, M., Gerez, C., Atta, M., & Jeunet, A. (1990) *Biochem. Biophys. Res. Commun. 168*, 659−664.
Guengerich, F. P. (1991) *J. Biol. Chem. 266*, 10019−10022.
Hagen, K. S., & Lachicotte, R. (1992) *J. Am. Chem. Soc. 114*, 8741−8742.
Kennedy, M. C., Gan, T., Antholine, W. E., & Petering, D. H. (1993) *Biochem. Biophys. Res. Commun. 196*, 632−635.
Kitajima, N., & Moro-oka, Y. (1994) *Chem. Rev. 94*, 737−757.
Kitajima, N., Tamura, N., Amagai, H., Fukui, H., Moro-oka, Y., Mizutani, Y., Kitagawa, T., Mathur, R., Heerwegh, K., Reed, C. A., Randall, C. R., Que, L., Jr., & Tatsumi, K. (1994) *J. Am. Chem. Soc. 116*, 9071−9085.
Kurtz, D. M., Jr. (1990) *Chem. Rev. 90*, 585−606.
Larsson, A., & Sjöberg, B.-M. (1986) *EMBO J. 5*, 2037−2040.
Lee, S.-K., Nesheim, J. C., & Lipscomb, J. D. (1993) *J. Biol. Chem. 268*, 21569−21577.
Lepoivre, M., Fieschi, F., Coves, J., Thelander, L., & Fontecave, M. (1991) *Biochem. Biophys. Res. Commun. 179*, 442−448.
Lepoivre, M., Flaman, J.-M., & Henry, Y. (1992) *J. Biol. Chem. 267*, 22994−23000.
Lepoivre, M., Flaman, J.-M., Bobé, P., Lemaire, G., & Henry, Y. (1994) *J. Biol. Chem. 269*, 21891−21897.
Ling, J., Nestor, L. P., Czernuszewicz, R. S., Spiro, T. G., Fraczkiewicz, R., Sharma, K. D., Loehr, T. M., & Sanders-Loehr, J. (1994a) *J. Am. Chem. Soc. 116*, 7682−7691.
Ling, J., Sahlin, M., Sjöberg, B.-M., Loehr, T. M., & Sanders-Loehr, J. (1994b) *J. Biol. Chem. 269*, 5595−5601.
Lynch, J. B. (1989) Ph.D. Thesis, University of Minnesota, Minneapolis, MN.
Lynch, J. B., Juarez-Garcia, C., Münck, E., & Que, L., Jr. (1989) *J. Biol. Chem. 264*, 8091−8096.
Magnus, K. A., Ton-That, H., & Carpenter, J. E. (1994) *Chem. Rev. 94*, 727−735.
Ménage, S., Zang, Y., Hendrich, M. P., & Que, L., Jr. (1992) *J. Am. Chem. Soc. 114*, 7786−7792.
Nelson, M. J. (1987) *J. Biol. Chem. 262*, 12137−12142.
Nocek, J. M., Kurtz, D. M., Jr., Sage, J. T., Xia, Y.-M., Debrunner, P., Shiemke, A. K., Sanders-Loehr, J., & Loehr, T. M. (1988) *Biochemistry 27*, 1014−1024.
Nordlund, P., & Eklund, H. (1993) *J. Mol. Biol. 232*, 123−164.
Nordlund, P., Sjöberg, B.-M., & Eklund, H. (1990) *Nature 345*, 393−398.
Orville, A. M., & Lipscomb, J. D. (1993) *J. Biol. Chem. 268*, 8596−8607.
Paul, P. P., & Karlin, K. D. (1991) *J. Am. Chem. Soc. 113*, 6331−6332.
Paul, P. P., Tyeklár, Z., Jacobson, R. R., & Karlin, K. D. (1991) *J. Am. Chem. Soc. 113*, 5322−5332.
Que, L., Jr. (1991) *Science 253*, 273−274.
Que, L., Jr., & True, A. E. (1990) *Prog. Inorg. Chem. 38*, 97−200.
Ravi, N., Bollinger, J. M., Jr., Huynh, B. H., Edmondson, D. E., & Stubbe, J. (1994) *J. Am. Chem. Soc. 116*, 8007−8014.
Reichard, P. (1993) *Science 260*, 1773−1777.
Sahlin, M., Sjöberg, B.-M., Backes, G., Loehr, T. M., & Sanders-Loehr, J. (1990) *Biochem. Biophys. Res. Commun. 167*, 813−818.
Salowe, S. P. (1987) Ph.D. Thesis, University of Wisconsin, Madison, WI.
Salowe, S. P., & Stubbe, J. (1986) *J. Bacteriol. 165*, 363−366.
Shiemke, A. K., Loehr, T. M., & Sanders-Loehr, J. (1986) *J. Am. Chem. Soc. 108*, 2437−2443.
Stenkamp, R. E. (1994) *Chem. Rev. 94*, 715−726.
Stubbe, J. (1990) *Adv. Enzymol. Relat. Areas Mol. Biol. 63*, 349−419.
Uhlin, U., & Eklund, H. (1994) *Nature 370*, 533−539.
Verplaaetse, J., van Tornout, P., Defreyn, G., Witters, R., & Lontie, R. (1979) *Eur. J. Biochem. 95*, 327−331.

BI950731P